Growing ZnO Crystals on Magnetite Nanoparticles

Rachel Turgeman, Shay Tirosh, and Aharon Gedanken*[a]

Abstract: We report herein on the oriented growth of ZnO crystals on magnetite nanoparticles. The ZnO crystals were grown by hydrolyzing a supersaturated aqueous solution of zinc nitrate. The seeds for the growth were magnetite nanoparticles with a diameter of 5.7 nm and a narrow size distribution. Hollowed ZnO hexagons of 0.15 μm width and 0.5 μm length filled with Fe_3O_4 particles were obtained. HR-TEM (high-resolution transmission electron microscopy) and selected-area EDS (energy-dispersive spectroscopy) show that the nanoparticles are homogenously spread in the ZnO tubes. Zeta potential measurements were employed to understand the relationship between the nanoparticles and the oriented growth of the ZnO crystals. The results show that the surfactants induced the directional growth of the ZnO crystals.

Keywords: crystal engineering · magnetite · nanostructures · zeta potential · zinc oxide

Introduction

ZnO is one of the important wide-band-gap materials (3.3 eV at 300 K). It is a low cost II-VI semiconductor, which is environmentally friendly and has superior electronic and optical properties. ZnO is currently in use, or being considered for use, as phosphors,[1] as component in electro-optical devices,[2–8] as piezoelectric transducers,[1,9,10] varistors,[1,11,12] UV and microwave absorbers,[1,10] gas sensors,[1,13,14,15] and for transparent conducting films.[1,16]

ZnO can be grown by means of a variety of techniques including vapor-phase transport,[18,19] sol–gel methods,[19,20] hydrothermal growth,[21,22] melt growth,[23] chemical vapor deposition (MOCVD),[24] electrochemical deposition,[25–28] laser ablation,[29] sputtering,[30] molecular beam epitaxy,[31,32] and spraying arc-discharge.[33]

However, large-scale use will require the development of simple, low-cost approaches. One such method is to grow ZnO from an aqueous solution at temperatures below 100 °C. The mild conditions of this synthesis allow the growth of ZnO by using surfactants[34–36] and diblock copolymers,[37,38] as well as the growth of ZnO on self-assembled monolayers (SAMs).[39,40] It was also found that diblock copolymers could play an important role in determining the morphology of $CaCO_3$[41,42] and $BaSO_4$.[43] Vayssieres and coworkers have also used the method described in references [34–40] for growing ZnO on various uncoated surfaces such as glass, Si wafers, ITO, and so forth.[44]

Crystal engineering by organic molecules mimics natural processes.[38,45] In natural processes, surfactant-like peptides and glycopeptides interact with nuclei and growing crystals.[46] This interaction is achieved by a combination of two factors, one of which is related to the chemical functional group, and the other to the structure, shape, orientation, and organization of the surfactants.

Previously, we studied crystal engineering of ZnO by growing the crystals on SAM of functionalized alkyl silane.[40] We have found that the monolayers deposited on a silicon wafer influence the orientation of ZnO crystal growth. The nature of the substituent and its organization affect the orientation of the ZnO growth. The current paper is an extension of previous work in which nanoparticles are used as seeds for the growth of the ZnO crystals. Nanoparticles of magnetite were selected as the seeds. One of the reasons for choosing the Fe_3O_4 nanoparticles as seeds is the existence of a very detailed and easy process for their preparation as monodispersed particles with narrow size distribution. In the preparation of the magnetite nanoparticles we have followed the process reported by Sun and Zeng.[47] They reported a simple organic-phase synthesis of magnetite nanoparticles with sizes variable from 3 to 20 nm in diameter. The 4 nm Fe_3O_4 nanoparticles are made by mixing $[Fe(acac)_3]$ in phenyl ether with 1,2-hexadecanediol, oleic acid, and oleylamine under nitrogen, and heating the mixture to reflux for 30 min. The product was dissolved in hexane in the presence of oleic acid and oleylamine, and reprecipitated with ethanol to give 4 nm Fe_3O_4 nanoparticles. The long alkyl chain coating prevents agglomeration of

[a] R. Turgeman, S. Tirosh, Prof. A. Gedanken
Department of Chemistry, Bar-Ilan University
Ramat-Gan, 52900 (Israel)
Fax: +(972) 5311250
E-mail: gedanken@mail.biu.ac.il

 DOI: 10.1002/chem.200306022

the magnetic particles, thus paving the way for obtaining monodispersed nanoparticles.

From our computer search it appears that the current investigation is the first attempt to grow oriented crystals on inorganic nanoparticles as seeds. We are aware that Wegner's group has grown ZnO crystals on 80–160 nm size latex particles.[48] The motivation of this study is first to understand the parameters of the nanoparticles that determine the crystal growth. The second reason, which is related specifically to magnetite, is the opportunity to expand the functionality of ZnO to magneto-optics as well as to spintronic devices, and so forth.

Results

Although we synthesized the nanosized Fe_3O_4 by the abovementioned procedure, with the same amount of each of the precursors, we did not observe X-ray diffraction for the products. This might be due to either the product being X-ray amorphous (i.e., smaller particles were obtained in our reaction than those in reference [47], or perhaps the temperature was lower than in the Sun report). The selected-area electron diffraction image (Figure 1) also indicated the

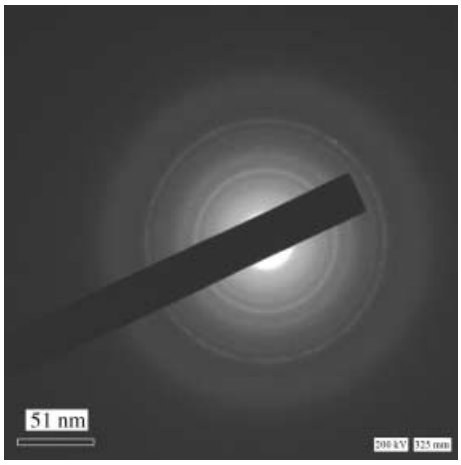

Figure 1. Electron diffraction pattern of magnetite nanoparticles.

amorphous nature of the product; a diffused ring pattern is detected. We therefore had to use other methods to characterize the product.

We have applied the spot test suggested by Feigel[49] to identify the presence of Fe^{2+} ions. Positive results were obtained when α,α′-phenantroline was added to the solution. The color was identical to that observed for commercial Fe_3O_4.

Mössbauer spectroscopy (MS) measurements also confirmed that the compound is amorphous. On the other hand, Fe_3O_4 crystals were positively identified by MS when the amorphous crystals were heated to the crystallization temperature determined by the DSC.

HR-TEM pictures of the magnetite nanoparticles are shown in Figure 2a and b. The size and size distribution

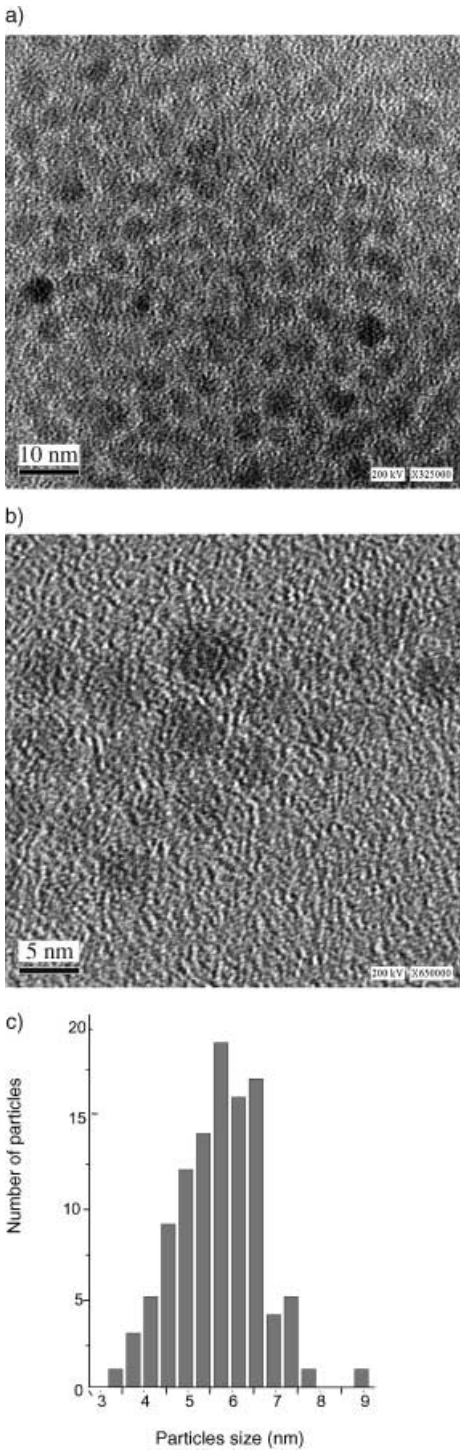

Figure 2. a) TEM micrographs of 5.7 nm Fe_3O_4 nanoparticles. b) High-magnification TEM micrograph, ×625 000. c) Particle-size histogram obtained from the HR-TEM data.

were determined from HR-TEM micrographs by measuring the diameters of 107 particles. The results of the particles size were plotted in a histogram, which is depicted in Figure 2c.

A statistical analysis of this histogram shows that the mean size of the nanoparticles is 5.7 ± 0.1 nm. The histogram reveals a narrow size distribution of particles, which according to the HR-TEM are monodispersed. The amor-

phous nature is also revealed in HR-TEM in which fringes are not detected for the as-prepared samples.

The surface area of these particles is less than 1 $m^2 g^{-1}$. This is a very small value for 5.7 nm particles and is attributed to the dense alkyl groups bonded to the particles' surface, hindering the passage of the nitrogen molecules to the magnetite surface.

The synthetic method used to grow the ZnO crystals was hydrolysis of a zinc nitrate solution. The ZnO crystals were grown on the magnetite nanoparticles by dispersing the particles in an aqueous solution that contains the zinc precursors. The process is described in greater detail elsewhere.[34–40]

HR-SEM (high-resolution scanning electron microscopy) micrographs of these crystals are shown in Figure 3. These pictures were compared to SEM pictures of a control

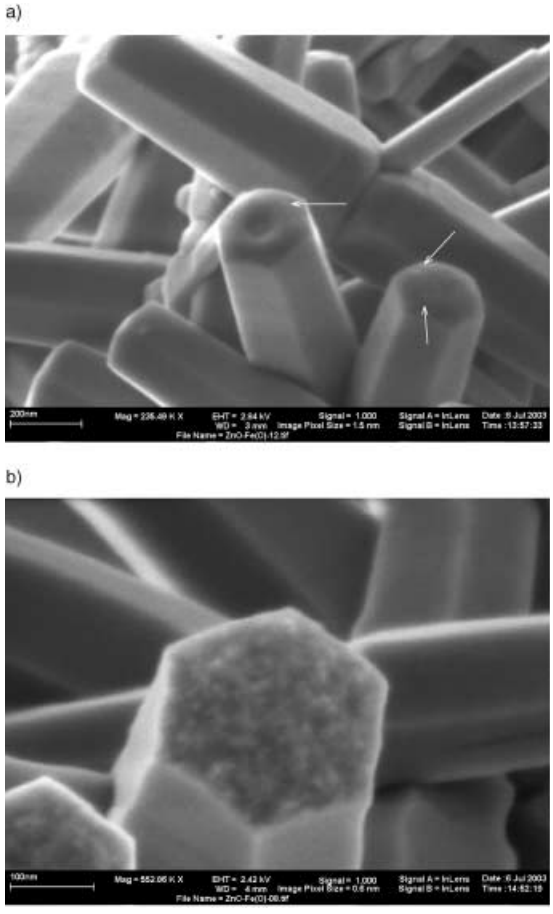

Figure 3. HR-SEM micrographs of the ZnO crystals that were grown on the magnetite nanoparticles: a) bar = 200 nm; b) bar = 100 nm. White arrows in a) show the (001) ZnO plane.

sample, namely, a sample of ZnO crystals that were grown in the absence of magnetite nanoparticles. This comparison showed that the size of the ZnO crystals that were grown on the particles decreased. The length of the crystals decreased from 3000 nm to 500 nm and the width decreased from 500 nm to 150 nm.

In Figure 3a, white arrows marked the (001) ZnO plane. A higher resolution picture is depicted in Figure 3b. The picture shows that the magnetite nanoparticles are encapsulated inside the ZnO crystal. SEM pictures of the reference sample showed that the ZnO crystals are not hollow. The planes of the ZnO crystals in the control experiments were much flatter than those grown on the magnetite nanoparticles.

Further measurements were employed in order to explore the homogeneity of the spreading of the nanoparticles in the hollowed ZnO crystal. This was done by selected-area EDS, through which we monitored the concentration of iron along the ZnO crystal. An equal amount of iron was found by measuring its quantity at three separate points along the ZnO tube.

By analyzing Figure 4, the embedded particle size was estimated to be in the range of 4–6 nm. The images in Figure 4a and b were measured at the head of the ZnO tube and those in Figure 4c and d were measured at the middle of the tube. This analysis shows that the embedded particles have the same size as the as-prepared magnetite nanoparticles. Second, the size of the embedded particles is uniform along the ZnO matrix.

The high-resolution TEM picture of a ZnO crystal lying on the grid perpendicular to the electronic beam and parallel to the horizontal plane of the grid is presented in Figure 4. Thus, fringes should be obtained only for the ZnO crystals.

We did not observe fringes in the magnetite nanoparticles due to their amorphous nature. On the other hand, the fringes of the ZnO walls are clearly observed in the three images, Figure 4b–d. The spacing measured between these fringes is 2. 83 Å. This fits very closely to the *d* value of the (100) planes.

The results of these experiments raise the question regarding the factors that determine the growth of the ZnO crystals. It is clear that due to the amorphous nature of the crystals, the Fe_3O_4 planes do not play an important role in determining the direction of the crystal growth. Our hypothesis was, therefore, directed towards the surfactant molecules and their organization as the determining factors of the growth.

The organization of two molecules with two different functional groups on a modified surface has been described previously for fatty acids and fatty amines.[50] Following this report and other studies about coating iron oxide with various surfactants,[51–53] we assume that the surfactant bilayer structure is as follows: The first layer consists of the oleic acid monolayer bound to the magnetite nanoparticles through ionic bonds (the COO^- is detected by IR spectroscopy). The outermost layer consists of an interdigitated monolayer of an alkylamine/alkylcarboxylic acid. Thus, acid–base moieties should be exposed in the outermost shell.

The coated magnetite particles form colloidal solutions in organic liquids. The as-prepared magnetite nanoparticles could be dispersed for short times in water as well. Dispersing the particles in an aqueous medium enabled us to conduct zeta potential measurements. We tried to follow the ZnO growth by measuring the zeta potential of particles in

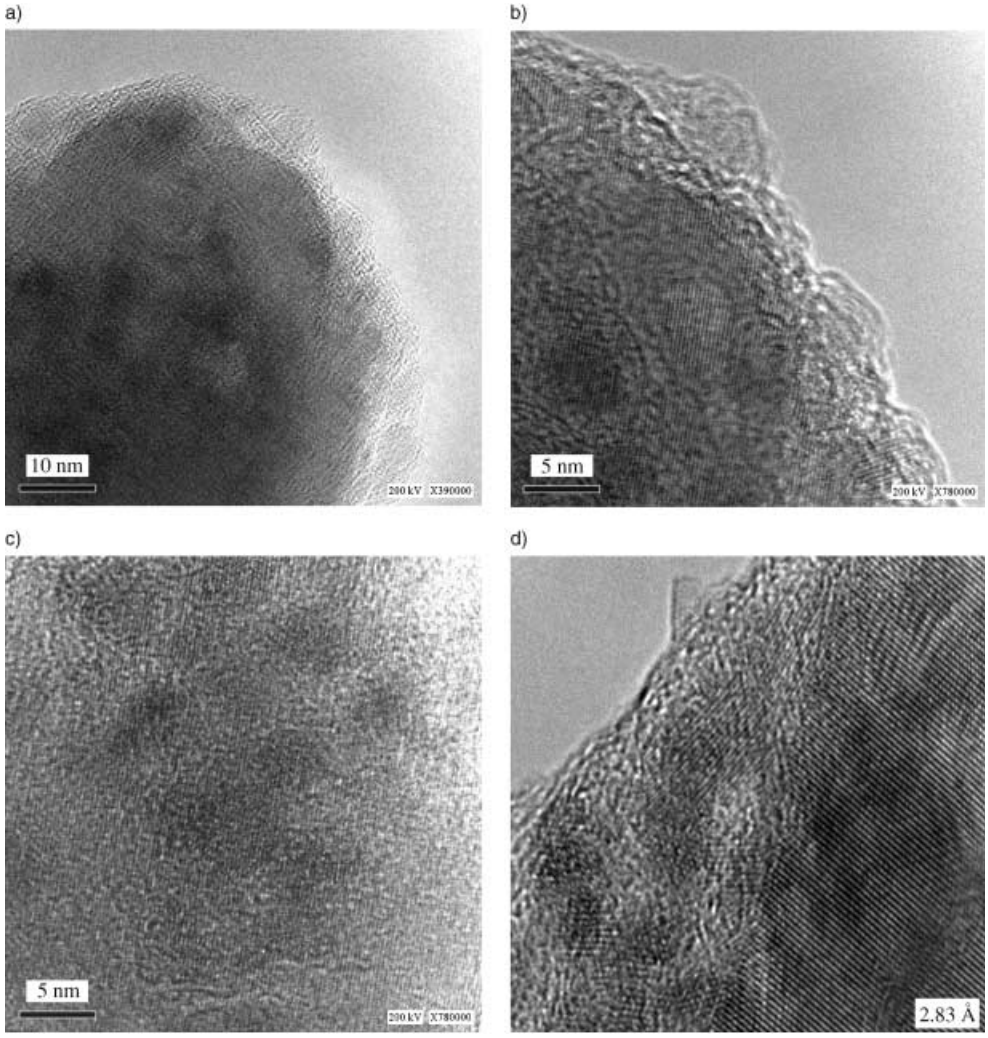

Figure 4. HRTEM micrographs of the ZnO grown on the magnetite nanoparticles. a) and b) show the embedded magnetite particles at the edge of the ZnO tube. c) and d) show the embedded magnetite at the middle of the tube.

the $Zn(NO_3)_2$ solution at pH of 5. Exposing the dispersed magnetite nanoparticles changed the zeta potential from -16.7 ± 1.7 mv to -2.9 ± 2.0 mv. The growth of ZnO occurs only when the pH of the solution is changed from 5 to 6. To probe whether the change in the zeta potential is due to the precipitating Zn^{2+} ions or to the changes in the pH, other experiments were conducted. We measured the zeta potential as a function of pH from 3 to 8 in the absence of Zn^{2+}. The pH was gradually changed from 3 to 8 by adding NaOH to the coated magnetite nanoparticles. The zeta potential decreased with the increase of pH in a titration-like shape. Special attention was dedicated to the pH change from 5 to 6. Almost no change in the zeta potential was recorded while the pH of solution changed from 5 to 6. Thus, we can conclude that the changes in the zeta potential upon the precipitation of the ZnO are not due to changes in the pH, but rather due to the adsorption of Zn^{2+} ions on the outer layer functional group of the surfactants. Indeed, the changes in the zeta potential indicate that the Zn^{2+} ions and not the O^{2-} or OH^- are first bonded to the surfactant double layer, and further dictate the directional growth of the ZnO crystal. It is clear from our HR-SEM pictures that the ZnO crystal grows along the *c* axis, a polar axis. Our results indicate that Zn^{+2} ions are firstly deposited on the outer layer of the surfactant and thus lead to the growth of the crystal along the *c* axis. The polar Zn surface (001) is not completed, because it contains magnetite particles at its center, and in this way supports the growth of the (100) planes.

Conclusion

HRTEM and zeta potential measurements show that the monodispersed magnetite nanoparticles function as seeds for ZnO crystal growth. The ability of these particles to fulfill this function is due to the terminated surfactant molecules of oleic acid and oleylamine.

The results of this report are very important, because it is the first report on the growth of crystals on monodispersed nanoparticles. Second, synthesizing a composite material of ZnO and magnetite nanoparticles will pave the way for ex-

panding the technological uses of ZnO. Further investigations on the influence of other surfactants on the growth of ZnO on various nanoprticles are in progress.

Experimental Section

Magnetite nanoparticle preparation: Iron(III) acetylacetonate (2 mmol) was mixed in phenyl ether (20 mL) with 1,2-hexadecanediol (10 mmol), oleic acid (6 mmol), and oleylamine (6 mmol) under nitrogen and heated to reflux for 30 min. After cooling to room temperature, the dark-brown mixture was treated with ethanol under air, and a dark-brown material was precipitated from the solution. The product was dissolved in hexane in the presence of oleic acid and oleylamine and reprecipitated with ethanol.

Crystallization of ZnO on nanoparticles: As-prepared magnetite nanoparticles (1 mg) were dispersed in deionzed water (100 mL). The dispersion was heated to 95 °C in a water-jacketed cell of 100 mL capacity. At this temperature, zinc nitrate ($Zn(NO_3)_2 \cdot 6H_2O$, Aldrich, 0.89 g) was dissolved in a very small amount of water and then added to the dispersion. The final concentration of the zinc nitrate solution was 0.03 M. This solution was heated for several minutes and then hexamethylene tetramine (Aldrich, HMT, 0.42 g) was dissolved in a very small amount of water. The final concentration of the HMT solution was 0.03 M. The high temperature was chosen in order to prevent the formation of zinc hydroxide, and lead to the decomposition of HMT to ammonia and formaldehyde. This caused a shift of the pH of the solution from 5 to around 6, which was the necessary basicity for the crystallization of ZnO. We stopped the crystallization after 45 min by cooling the vessel to room temperature. After the ZnO crystallization, the reaction solution was centrifuged and washed with water and ethanol several times, and then dried in vacuum at room temperature overnight.

Apparatus: HR-TEM images were taken using a JEOL 3010 model with 300 kV accelerating voltage. A conventional monochrome CCD camera, with a resolution of 768×512 pixels, was used to digitize the images. The digital images were processed with the Digital Micrograph software package (Gantan, Pleasanton, CA, USA). Samples for TEM were prepared by placing a drop of the sample suspension on a copper grid (400 mesh, Electron Microscope Sciences) coated with carbon film.

Selected-area EDS and selected-area electron diffraction measurements were conducted with the HRTEM instrument, while the size of electron beam was reduced to 35 nm.

HR-SEM images were taken with a SUPRA 55 VP FEG LEO. Zeta potential measurements were carried out with a Malvern zetasizer 3000 HSA (High Resolution Analysis).

Acknowledgement

The authors gratefully acknowledge the support of the Germany–Israel Program (DIP) of the German DLR. The authors also thank Dr. K. Gartzman, the Weizmann Institute (Israel), Mr. L. Grossman, B. G. Technical Support, and Dr. H. Jaksch of the LEO GEMINI company for conducting HR-SEM measurements on their LEO SUPRA 55 VP instruments.

[1] D. C. Look, *Mater. Sci. Eng.* **2001**, *80*, 383–387.
[2] *Thin Film Solar Cells* (Eds.: K. L. Chopra, S. R. Das), Plenum, New York, **1983**.
[3] H. Karzel, W. Potzel, M. Kofferlein, W. Schiessl, M. Steiner, U. Hiller, G. M. Kalvius, D. W. Mitchell, T. P. Das, P. Blaha, K. Schwarz, M. P. Pasternak, *Phys. Rev.* **1996**, *53*, 11425–11438.
[4] S. Cho, J. Ma, Y. Kim, Y. Sun, G. K. L. Wong, J. B. Ketterson, *Appl. Phys. Lett.* **1999**, *75*, 2761–2763.
[5] L. B. Kong, F. Li, Y. Zhang, X. Yao, *J. Mater. Sci. Lett.* **1998**, *17*, 769–771.
[6] W. C. Shih, M. S. Wu, *J. Cryst. Growth* **1994**, *137*, 319–325.
[7] C. T. Troy, *Photonics Spectra* **1997**, *31*, 34–34.
[8] K. Vanheusden, C. H. Seager, W. L. Warren, D. R. Tallant, J. Caruso, M. J. Hampden Smith, T. T. Kodas, *J. Lumin.* **1997**, *75*, 11–16.
[9] *Comprehensive Inorganic Chemistry* (J. C. Bailar, H. J. Emele'us, R. Nyholm, A. F. Trotman-Dickenson), Pergamon, Oxford, **1973**.
[10] A. R. Hutson, *Phys. Rev. Lett.* **1960**, *4*, 505–507.
[11] T. K. Gupta, *J. Am. Ceram. Soc.* **1990**, *73*, 1817–1840.
[12] J. Lee, J. H. Hwang, J. J. Mashek, T. O. Mason, A. E. Miller, R. W. Siegel, *J. Mater. Res.* **1995**, *10*, 2295–2300.
[13] Z. C. Jin, I. Hamberg, C. G. Granqvist, B. E. Sernelius, K. F. Berggren, *Thin Solid Films* **1988**, *164*, 381–386.
[14] A. P. Chatterjee, P. Mitra, A. K. Mukhopadhyay, *J. Mater. Sci.* **1999**, *34*, 4225–4231.
[15] T. Seiyama, A. Kato, K. Fujiishi, M. Nagatani, *Anal. Chem.* **1962**, *34*, 1502–1503.
[16] M. J. Brett, R. R. Parsons, *Solid State Commun.* **1985**, *54*, 603–606.
[17] A. Urbieta. P. Fernandez, C. Hardalov, J. Piqueras, T. Sekiguchi, *Mater. Sci. Eng.* **2002**, *91/92*, 345–348.
[18] D. C. Look, D. C. Reynolds. J. R. Sizelove, R. L. Jones, C. W. Litton, G. Cantwell, W. C. Harsch, *Solid State Commun.* **1998**, *105*, 399–401.
[19] N. Takahashi, K. Kaiya, K. Omichi, T. Nakamura, S. Okamoto, H. Yamamoto, *J. Cryst. Growth* **2000**, *209*, 822–827.
[20] L. Spanhel, M. A. Anderson, *J. Am. Chem. Soc.* **1991**, *113*, 2826–2833.
[21] M. Suscavage, M. Harris, D. Bliss, P. Yip, S. Q. Wang, D. Schwall, L. Bouthillette, J. Bailey, M. Callahan, D. C. Look, D. C. Reynolds, R. L. Jones, C. W. Litton, *MRS Internet J. Nitride Semicond. Res.* **1999**, *4*, G 3.40, Suppl. 1.
[22] E. V. Kortounova, Lyutin, V. I. *Ann. Chim. Sci. Mater.* **1997**, *22*, 647–650.
[23] J. Nause, *III-Vs Rev.* **1999**, *12*, 28–31.
[24] J. S. Kim, H. A. Marzouk, P. J. Reucroft, C. E. Hamrin, *Thin Solid Films* **1992**, *217*, 133–137.
[25] I. Masanobu, O. Takashi, *Appl. Phys. Lett.* **1996**, 68, 2439–2440.
[26] S. Peulon, D. Lincot, *J. Electrochem. Soc.* **1998**, *145*, 864–874.
[27] T. Yoshida, M. Tochimoto, D. Schlettwein, D. Wohrle, T. Sugiura, H. Minoura, *Chem. Mater.* **1999**, *11*, 2657–2667.
[28] B. O'Regan, D. T. Schwartz, S. M. Zakeeruddin, M. Gratzel, *Adv. Mater.* **2000**, *12*, 1263–1267.
[29] H. K. Ardakani, *Thin Solid Films* **1996**, *287*, 280–283.
[30] A. Valentini, F. Quaranta, M. Penza, F. R. Rizzi, *J. Appl. Phys.* **1993**, *73*, 1143–1145.
[31] Y. F. Chen, D. M. Bagnall, H. J. Koh, K. T. Park, K. Hiraga, Z. Q. Zhu, T. Yao, *J. Appl. Phys.* **1998**, *84*, 3912–3918.
[32] Y. F. Chen, D. M. Bagnall, Z. Q. Zhu, T. Sekiuchi, K. T. Park, K. Hiraga, T. Yao, S. Koyama, M. Y. Shen, T. Goto, *J. Cryst. Growth* **1997**, *181*, 165–169.
[33] M. Kitano, T. Hamabe, S. Maede, *J. Cryst. Growth* **1993**, *128*, 1099–1103.
[34] L. Guo, L. Y. Ji, H. Xu, *J. Am. Chem. Soc.* **2002**, *124*, 14864–14865.
[35] Z. R. Tian, J. A. Voigt. B. McKenzie, J. M. McDermott, *J. Am. Chem. Soc.* **2002**, *124*, 12954–12955.
[36] K. S. Choi, H. C. Lichtenegger, G. D. Stucky, *J. Am. Chem. Soc.* **2002**, *124*, 12402–12403.
[37] R. V. Kumar, R. Elgamiel, Y. Koltypin, J. Norwig, A. Gedanken, *J. Cryst. Growth* **2003**, *250*, 409–417.
[38] M. Öner, J. Norwig, W. H. Meyer, G. Wegner, *Chem. Mater.* **1998**, *10*, 460–463.
[39] M. R. De Guire, T. P. Niesen, S. Supothina, J. Wolff, J. Bill, C. N. Sukenik, F. Aldinger, A. H. Heuer, M. Ruhle, *Z. Metallkd.* **1998**, *89*, 758–766.
[40] R. Turgeman, O. Gershevitz, O. Palchik, M. Deutsch, B. M. Ocko, A. Gedanken, C. N. Sukenik, *Cryst. Growth Des.* **2004**, *4*, 169–175.
[41] J. M. Marentette, J. Norwig, E. Stöckelmann, W. H. Meyer, G. Wegner, *Adv. Mater.* **1997**, *9*, 647–651.
[42] H. Colfen, M. Antonietti, *Langmuir* **1998**, *14*, 582–589.
[43] Q. Limin, H. Colfen, M. Antonietti, *Chem. Mater.* **2000**, *12*, 2392–2403.
[44] L. Vayssieres, K. Keis, S.-E. Lindquist, A. Hagfeldth, *J. Phys. Chem. B* **2001**, *105*, 3350–3352.

[45] M. Seldak, M. Antonietti, H. Colfen, *Macromol. Chem. Phys.* **1998**, *199*, 247–254.
[46] *Dahlem Workshop on Biological Mineralization and Demineraliazation* (G. H. Nancollas), Springer, Berlin, **1982**.
[47] S. Sun, H. Zeng, *J. Am. Chem. Soc.* **2002**, *124*, 8204–8205.
[48] G. Wegner, P. Baum, M. Muller, J. Norwig, K. Landfester, *Macromol. Symp.* **2001**, *175*, 349–355
[49] F. Feigel, *Spot Tests, Inorganic Applications, Vol. 1*, Elsevier, New York, **1954**, pp. 154–155.
[50] M. Sastry, M. Rao, K. M. Ganesh, *Acc. Chem. Res.* **2002**, *35*, 847–855.
[51] L. Fu, V. P. Dravid, D. L. Johnson, *Appl. Surf. Sci.* **2001**, *181*, 173–178.
[52] L. Shen, P. E. Laibinis, T. A. Hatton, *Langmuir* **1999**, *15*, 447–453.
[53] G. Kataby, M. Cojocaru, R. Prozorov, A. Gedanken, *Langmuir* **1999**, *15*, 1703–1708.

Received: December 14, 2003 [F6022]